Formation, evolution and photoluminescence properties of Si nanoclusters

2007 J. Phys.: Condens. Matter 19 225003

(http://iopscience.iop.org/0953-8984/19/22/225003)

IOP PUBLISHING JOURNAL OF PHYSICS: CONDENSED MATTER

J. Phys.: Condens. Matter **19** (2007) 225003 (24pp) doi:10.1088/0953-8984/19/22/225003

Formation, evolution and photoluminescence properties of Si nanoclusters

Simona Boninelli[1], Fabio Iacona[2,3], Giorgia Franzò[1], Corrado Bongiorno[2], Corrado Spinella[2] and Francesco Priolo[1]

[1] MATIS CNR-INFM and Dipartimento di Fisica e Astronomia, Università di Catania, via Santa Sofia 64, I-95123 Catania, Italy
[2] CNR-IMM, Sezione di Catania, stradale Primosole 50, I-95121 Catania, Italy

E-mail: fabio.iacona@imm.cnr.it

Received 11 July 2006, in final form 24 July 2006
Published 14 May 2007
Online at stacks.iop.org/JPhysCM/19/225003

Abstract

Si nanoclusters embedded in SiO_2 have been produced by thermal annealing in the 900–1250 °C range of SiO_x films or of SiO_2/Si/SiO_2 multilayers, both prepared by plasma enhanced chemical vapour deposition. The structural properties of these systems have been investigated by energy filtered transmission electron microscopy. This technique, due to its capability to detect Si nanoclusters independently of the presence of a crystalline phase, has evidenced a relevant contribution of amorphous nanostructures, not detectable by using the more conventional dark field transmission electron microscopy technique. By also taking into account this contribution, an accurate quantitative description of the evolution of the samples upon thermal annealing has been accomplished. The temperatures at which the formation of amorphous and crystalline Si nanoclusters starts have been determined. Furthermore, the nanocluster mean radius and density and the crystalline fraction have been determined as a function of the annealing temperature. Finally, the optical and the structural properties of the two systems have been compared, leading to the demonstration that the photoluminescence properties are determined by both the amorphous and crystalline clusters.

1. Introduction

Si nanocrystals (ncs) are currently the most promising approach to turn Si, an indirect energy bandgap material, into an efficient light emitter. Indeed, the bandgap of Si ncs is enlarged with respect to the bulk material due to quantum confinement effects, and an intense visible photoluminescence (PL) at room temperature is obtained. Major advancements towards the application of this material in optoelectronics have been recently represented by the observation

[3] Author to whom any correspondence should be addressed.

of light amplification in Si ncs [1–7], as well as by the fabrication of efficient light emitting devices based on Si ncs [8–16].

Among the different techniques used for Si nc synthesis, the high temperature annealing of substoichiometric silicon oxide (SiO_x) films prepared by plasma enhanced chemical vapour deposition (PECVD) or sputtering exhibits a lot of advantages [17–22]. These processes are indeed highly compatible with the Si VLSI technology and produces stable (Si ncs are embedded into a SiO_2 layer) and efficient light emitters. Furthermore, the Si nc size can be controlled by changing the annealing temperature as well as the silicon excess in the SiO_x film; in addition, it has been observed that by increasing the Si nc mean size a red-shift of the PL peak is obtained, in qualitative agreement with the quantum confinement model. PECVD and sputtering can also be successfully used for the preparation of Si/SiO_2 superlattices [23–27]. When these systems are annealed at high temperature Si nc formation occurs [25]. The PL emission from these materials presents some peculiarities related to the ordered arrangement of the emitting centres [25].

A key point for a full understanding of the optical properties of the above described systems is the availability of a clear picture of their structural properties and their evolution upon thermal annealing. Under this respect, several techniques have been proposed for Si nc characterization, namely transmission electron microscopy (TEM) [20–27], x-ray diffraction (XRD) [23, 26] and Raman spectroscopy [20, 23]. All of these techniques are able to estimate the Si nc mean radius. In particular, reliable measurements of the Si nc size have been obtained by TEM analysis (from dark field or high resolution measurements). This technique, however, is not able to give a complete quantitative picture of the system, missing a fundamental information such as the Si nc density. Furthermore, all of these techniques are almost blind to the presence of amorphous Si clusters. As a consequence, an exhaustive correlation between the density and the size of the Si nanoclusters and the PL properties of the system is still lacking. Finally, the actual contribution given by amorphous clusters to the optical properties of the system is not fully understood yet.

In this work we will review our recent work on the structural and optical evolution of SiO_x films prepared by PECVD, upon thermal annealing processes up to 1250 °C. The early stages of the separation of the Si and SiO_2 phases, the formation of amorphous Si clusters and their transition to the crystalline phase have been investigated in detail by energy filtered transmission electron microscopy (EFTEM). The presence of a relevant contribution of Si amorphous nanostructures, not detectable by using the conventional dark field TEM (DFTEM) technique, has been demonstrated. By taking this contribution into account, an accurate quantitative description of the nanostructure formation process has been accomplished, and the mean size and the density of the Si clusters have been determined as a function of the annealing temperature. In addition, we will present data on the thermal evolution of a single, ultra-thin (3 nm) Si layer sandwiched between two thin SiO_2 layers (7 nm). It has been demonstrated that the first stages of the thermal evolution of the Si layer involve the formation of a highly interconnected Si network, followed by the appearance of well defined nanoclusters (both amorphous and crystalline). Also in this case the quantitative analysis of the EFTEM data has allowed the determination of the Si nanocluster size and density, as well as of their crystalline fraction. Finally, for both systems it will be demonstrated that the PL emission is quantitatively related to the density and size of the sum between amorphous and crystalline Si nanoclusters.

2. Experimental details

SiO_x thin films have been prepared by using a parallel plate PECVD system, consisting of an ultra-high vacuum chamber (base pressure 1×10^{-9} Torr) and an rf generator (13.56 MHz),

connected through a matching network to the top electrode of the reactor; the bottom electrode is grounded and also acts as sample holder. Deposition processes have been performed by using 50 W of input power. The substrates, consisting of Si wafers, have been heated at 300 °C during the deposition. The source gases used are high purity (99.99% or higher) SiH_4 and N_2O; the N_2O/SiH_4 flow ratio has been set to give SiO_x films with a total Si concentration of 46 at.%, as determined by Rutherford backscattering spectrometry (RBS) measurements. The total pressure during the deposition processes was about 8×10^{-2} Torr. The film thickness was about 80 nm.

$SiO_2/Si/SiO_2$ multilayers were deposited on Si substrates heated at 300 °C by using the same PECVD system as described above. SiO_2 layers were deposited by using a SiH_4 flow rate of 1 sccm and a N_2O flow rate of 30 sccm, with a total pressure of 3.5×10^{-2} Torr and 30 W of rf power. Si layers were deposited by using a SiH_4 flow rate of 20 sccm, with a total pressure of 1.5×10^{-2} Torr and 25 W of rf power. The thickness of the layers was about 7 nm for SiO_2 and about 3 nm for Si. The same conditions have been used for the synthesis of ten-period Si/SiO_2 multilayers, to be used for PL measurements.

After deposition, the films have been annealed at temperatures ranging between 900 and 1250 °C and for times ranging between 0.5 and 16 h in ultra-pure N_2 atmosphere by using a horizontal furnace. The rapid processes used in some of the experiments have been performed in a rapid thermal annealing apparatus.

Room temperature PL measurements were performed by pumping with the 488 nm line of an Ar^+ laser. The pump power was varied in the range of 10–50 mW over a circular area of about 1 mm in diameter and the laser beam was chopped by an acousto-optic modulator. The PL signal was analysed by a single grating monochromator and it was detected either by a photomultiplier tube or by a liquid nitrogen cooled Ge detector. Spectra were recorded with a lock-in amplifier synchronized to the acousto-optic modulator. All spectra have been corrected for the detector response. PL lifetime measurements were performed by chopping the laser beam with an acousto-optic modulator, detecting the PL signal with a photomultiplier tube and analysing it with a photon counting multichannel scaler having the signal from the modulator as a trigger. The overall time resolution of the system is $\sim$30 ns.

The Si nanocluster formation was monitored by using a 200 kV JEOL JEM 2010F energy filtered transmission electron microscope equipped with a Gatan Image Filter. This system consists of a conventional TEM coupled with an electron energy loss spectrometer. Si maps have been obtained by using a 4 eV wide energy window centred in correspondence to the Si plasmon loss peak at about 17 eV. The same microscope has also been used to collect dark field TEM images, by selecting a small portion (about 10%) of the diffraction ring of the (111) Si planes, and bright field images.

3. Results and discussion

3.1. Si nanoclusters from SiO_x films

The EFTEM technique is able to generate a TEM image by using only electrons that have lost a specific amount of energy due to the interaction with the sample. This allows us to obtain a chemical mapping of all the elements with the very high spatial resolution typical of TEM and therefore represents a particularly suitable method to detect silicon nanoclusters (both crystalline and amorphous and independently of the crystal orientation with respect to the incident electron beam) dispersed in a silica matrix.

The first step to obtain an energy filtered image is the use of electron energy loss spectroscopy (EELS) to collect an energy loss spectrum. EELS concerns the analysis of the energy spreading of initially almost monoenergetic electrons, after their interaction with the

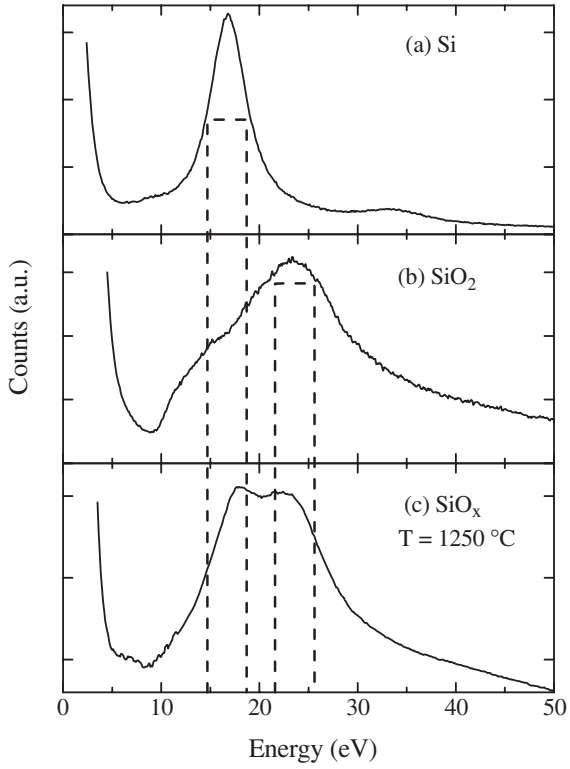

Figure 1. EELS spectra relative to (a) crystalline silicon, (b) amorphous silicon dioxide, and (c) SiO_x after a thermal annealing at 1250 °C. For all spectra, the zero loss peak is not fully plotted. Also in the figure the energy windows we have used to generate the EFTEM images reported in the remainder of the paper are shown.

sample. Fast electrons passing through the matter experience a great number of scattering events. A fraction of transmitted electrons does not suffer any energy loss (elastic scattering). Elastic scattering provides the most important contribution to the contrast in conventional TEM images. On the other hand, in the EELS technique the energy spectrum of the electrons is analysed, paying attention to the inelastically scattered electrons, that have suffered energy loss processes.

Figure 1 reports the EELS spectrum of a SiO_x film annealed at 1250 °C for 1 h. For comparison, the spectra obtained from reference c-Si and SiO_2 are also shown. In the figure we report the EELS spectra in the 0–50 eV range, dominated by the plasmon loss peaks, due to the excitation of collective vibrational modes of valence electrons, and by the zero-loss peak, due to electrons that have been elastically scattered or transmitted without any scattering event. At higher energy loss the intensity of the spectrum dramatically falls, but superposed on this decline weak signals due to the Si and O ionization edges emerge, due to the excitation of core electrons to an unoccupied electronic state above the Fermi level. From the analysis of the figure we note that the Si and SiO_2 plasmon peaks are centred, respectively, at about 17 and 23 eV. On the other hand, the spectrum relative to the SiO_x sample annealed at 1250 °C presents two well resolved components, whose energies correspond to the Si and SiO_2 plasmon losses. This is clear evidence of the extensive phase separation induced by the high temperature annealing in SiO_x films.

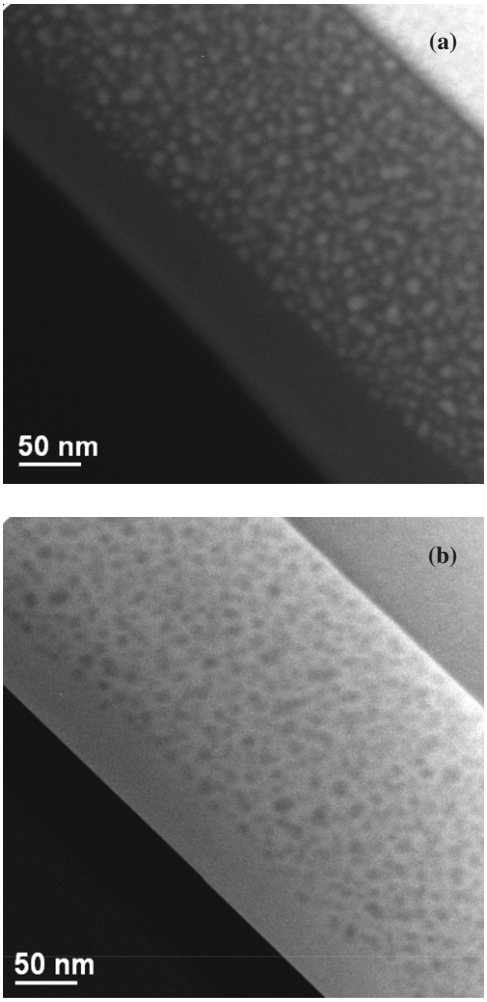

Figure 2. EFTEM cross section images of a SiO_x film annealed at 1250 °C obtained by selecting (a) Si or (b) SiO_2 plasmon loss electrons by means of the energy windows schematically depicted in figure 1.

By applying the EFTEM technique, it is possible to form a TEM image by selecting energy loss electrons with an energy window centred in correspondence to a given feature of the EELS spectrum. In our case, to map the presence of Si nanoclusters formed inside a SiO_x layer by a thermal annealing process, we put a 4 eV wide energy window in correspondence to the Si plasmon loss (17 eV). Conversely, to obtain a chemical mapping of the oxide we fixed the energy window at 23 eV. The energy shift of 6 eV between the Si and SiO_2 plasmon peaks allows us to neatly discriminate the two contributions and to realize energy filtered images by selecting plasmon loss electrons. As an example, we report in figure 2 two cross section EFTEM images of a SiO_x film annealed at 1250 °C, taken by selecting respectively the Si and SiO_2 plasmon loss electrons. This implies that in figure 2(a) the bright spots are Si nanoclusters while the dark regions correspond to the SiO_2 matrix; in a complementary way, in figure 2(b) the bright background is due to the presence of silica while the dark spots are the nanoclusters.

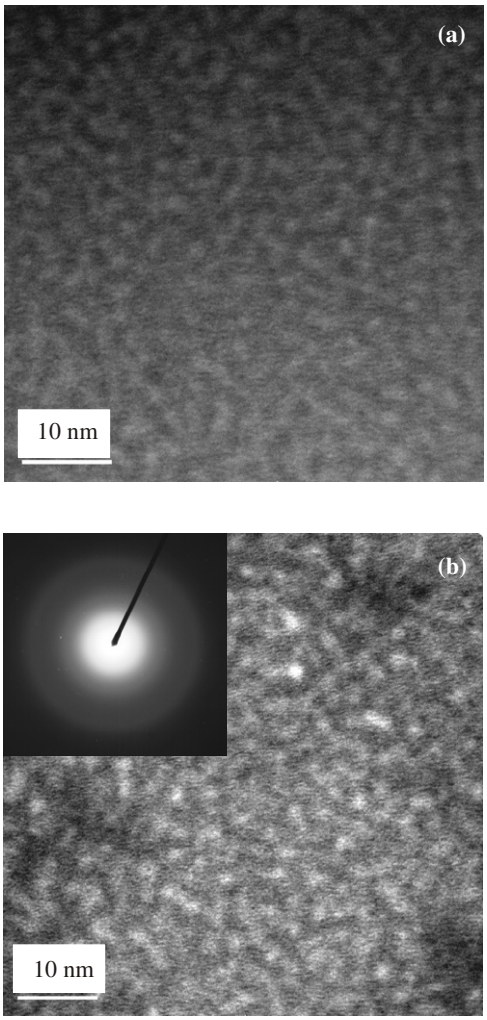

Figure 3. EFTEM plan view images obtained from SiO_x films annealed for 1 h at (a) 900 °C and (b) 1000 °C. The bright zones reveal the presence of Si clusters. The inset of (b) shows the electron diffraction pattern of the sample annealed at 1000 °C.

EFTEM images can be also obtained by using the ionization edges (and in particular the L edge of silicon at about 100 eV and the K edge of oxygen at about 530 eV). However, from the practical point of view, since the value of the cross section for plasmon interaction is about one order of magnitude higher than that due to core–shell ionization [28], the use of plasmon losses provides the most suitable method for collecting EFTEM images with a high signal-to-noise ratio.

We have used the EFTEM technique to monitor the formation and growth of Si nanoclusters from annealed SiO_x samples. Plan view images have been obtained by using an energy window in correspondence to the Si plasmon loss. The EFTEM analysis of an as deposited SiO_x sample shows a uniform background without any appreciable intensity contrast, demonstrating the absence of any phase separation effect. On the other hand, in the EFTEM image reported in figure 3(a), referring to a sample annealed at 900 °C for 1 h, some brighter

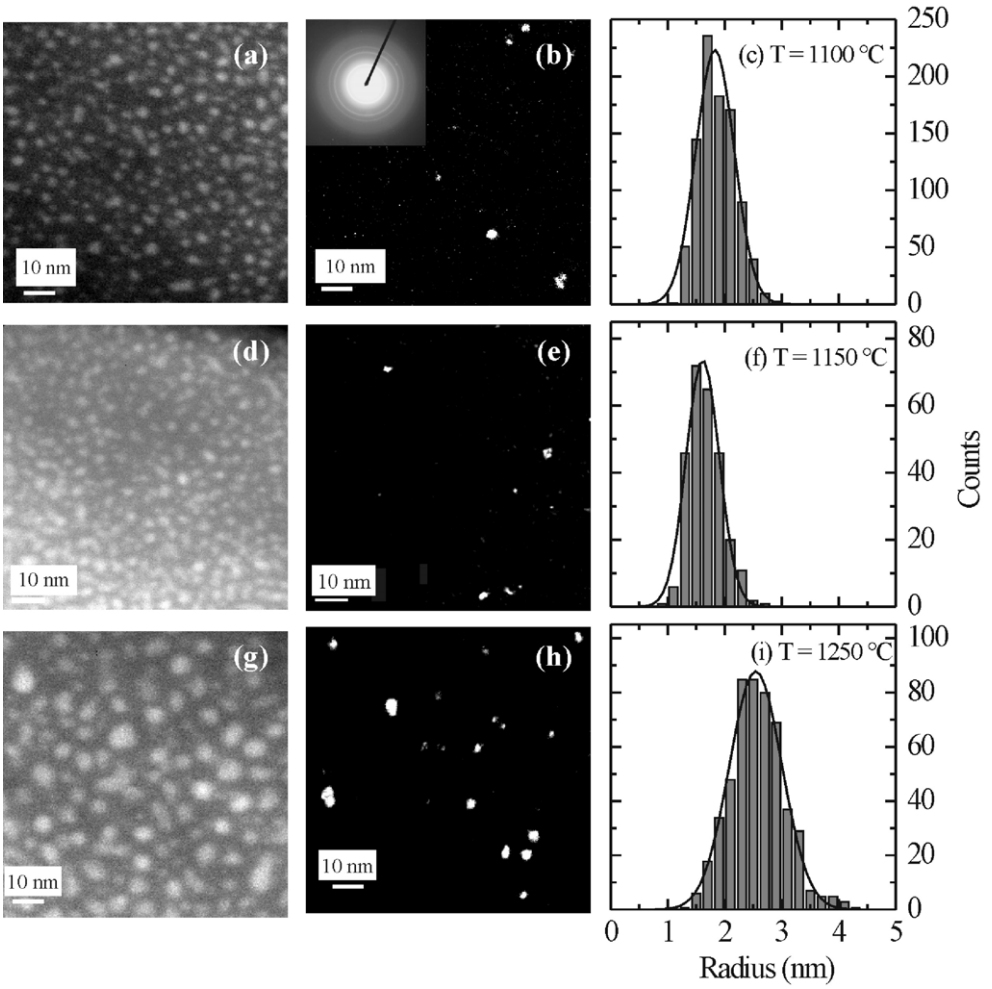

Figure 4. EFTEM plan view images ((a) 1100 °C, (d) 1150 °C, (g) 1250 °C), DFTEM plan view images ((b) 1100 °C, (e) 1150 °C, (h) 1250 °C) and Si nanocluster size distributions obtained from the analysis of the EFTEM images ((c) 1100 °C, (f) 1150 °C, (i) 1250 °C) obtained from SiO_x films annealed for 1 h. The inset of (b) shows the electron diffraction pattern of the sample annealed at 1100 °C.

zones can be clearly detected. This means that clustering effects are already visible at 900 °C, even if the image seems to suggest the formation of a Si network instead of isolated clusters. The occurrence of a phase separation between Si and SiO_2 becomes much more evident by increasing the annealing temperature, and well defined Si clusters embedded in the oxide matrix are clearly visible in the sample annealed at 1000 °C (see figure 3(b)).

To gain a deeper knowledge of the structural properties of these systems, we have employed the more conventional DFTEM technique. It is well known that this technique is sensitive to the presence of crystalline planes, and it is therefore able to map the system for the presence of crystalline Si clusters. On the other hand, we remark again that the EFTEM images reported in figure 3 have to be considered as chemical maps, the Si clusters being detected independently of their crystalline structure. In agreement with literature data [21], it

was not possible to observe any diffraction pattern corresponding to the presence of a crystalline phase for samples as deposited and annealed at 900 and 1000 °C; indeed the diffraction pattern reported in the inset of figure 3(b) presents only the characteristic broad ring observed in the presence of an amorphous phase. We can therefore conclude that all the clusters shown in figures 3(a) and (b) are amorphous.

On the other hand, the samples annealed at temperatures of 1100 °C or higher exhibit a diffraction pattern, shown in the inset of figure 4(b), mainly consisting of three well distinct rings corresponding to the (111), (220) and (311) planes of c-Si, indicating the formation of Si ncs. The direct comparison between energy filtered and dark field images is shown in figure 4 for samples annealed at temperatures of 1100 ((a) and (b)), 1150 ((d) and (e)) and 1250 °C ((g) and (h)). The dark field plan view TEM images, shown in figures 4(b), (e) and (h), have been obtained by selecting a small portion (about 10%) of the diffraction ring due to the (111) Si planes, while the energy filtered images shown in figures 4(a), (d) and (g) have been collected again by mapping the presence of Si clusters through the use of an energy window centred in correspondence to the Si plasmon loss. In dark field images, Si ncs appear as bright spots on a dark background. Direct comparison between images obtained with the two different techniques on the same sample clearly demonstrates that energy filtered images, due to their capability to show all the Si clusters, allow a much more complete characterization if compared with the dark field technique, showing only a small portion of the crystalline population.

A qualitative analysis of the TEM images shown in figures 3 and 4 allows us to define some aspects of the Si nanocluster nucleation from annealed SiO_x films. As deposited SiO_x films are homogeneous and fully amorphous materials, without any evidence of phase separation between Si and SiO_2. This is in agreement with the description of SiO_x films given by the random bonding model (RBM) [29], that we can reasonably assume to describe as deposited films, since they have been deposited at low temperature (300 °C). The first stages of the phase separation between Si and SiO_2 become visible at 900 °C, but well defined and amorphous Si clusters are formed only at 1000 °C. At 1100 °C the amorphous nanoclusters (na) begin to become crystalline. We remark here that this general behaviour has to be considered valid for any SiO_x composition; on the other hand, the clustering and crystallization temperatures we have determined (1000 and 1100 °C, respectively) exactly apply only to the Si concentration we used for the experiments reported in the present paper (46 at.%), since lower temperatures are expected when dealing with SiO_x films characterized by higher Si concentrations [21, 30].

Quantitative information on the annealed SiO_x samples can be obtained by measuring the radius of the Si nanoclusters detected in both energy filtered and dark field plan view images. A threshold value of 0.7 nm for the smallest significant radius has been used. The cluster radii have been plotted in the form of a histogram, reporting the frequency count for all the different detected sizes, grouped in bins having a width of 0.2 nm. Histograms have been fitted with Gaussian curves to extract a mean radius. Size distributions are characterized by a standard deviation of about 20%. The histograms showing the size distribution of the cluster detected by EFTEM for SiO_x samples annealed at 1100, 1150 and 1250 °C are reported in figures 4(c), (f) and (i) respectively. The mean radius of the Si clusters, as obtained by using both the EFTEM and DFTEM techniques, is reported in figure 5 as a function of the annealing temperature. Both techniques agree in demonstrating that the mean radius increases by increasing the annealing temperature, but values obtained from EFTEM data are systematically larger than those obtained from the dark field images.

A possible explanation for this discrepancy has been obtained by collecting high resolution EFTEM images. An example is shown in figure 6, referring to a Si nc detected in a SiO_x film annealed at 1250 °C. The image evidences that the lattice planes of crystalline Si are only visible in half of the cluster, probably due to the presence of a defect, bringing the

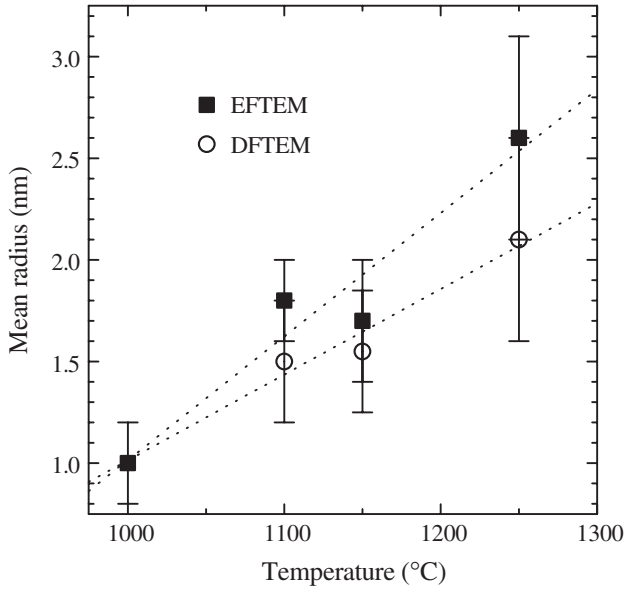

Figure 5. Si nanocluster mean radius, obtained from EFTEM and DFTEM images, as a function of the annealing temperature. The lines are drawn to guide the eye.

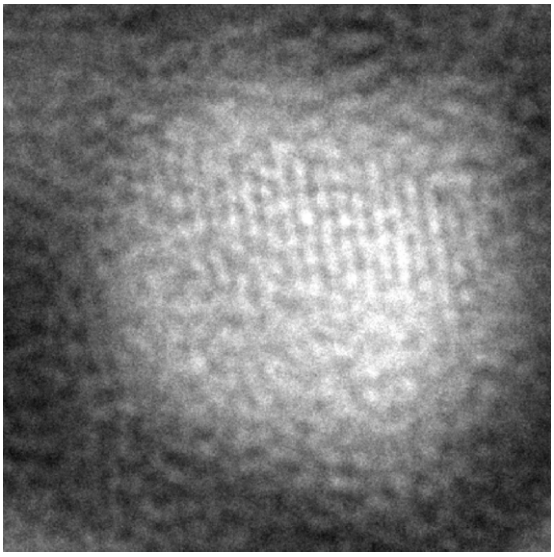

Figure 6. High resolution EFTEM images of a Si nc formed by thermal annealing at 1250 °C of a SiO_x film. Note the complete absence of lattice planes in half of the Si nanocluster.

other part of the nc off Bragg condition. Obviously, when looking at such a type of nc by using a conventional dark field analysis, only the part in the Bragg condition is visible, and this leads to an underestimation of its size. Another reason for the underestimation of the Si nc size by the DFTEM technique may be represented by the presence of an amorphous Si shell for a significant fraction of Si nanoclusters. High resolution EFTEM images have indeed

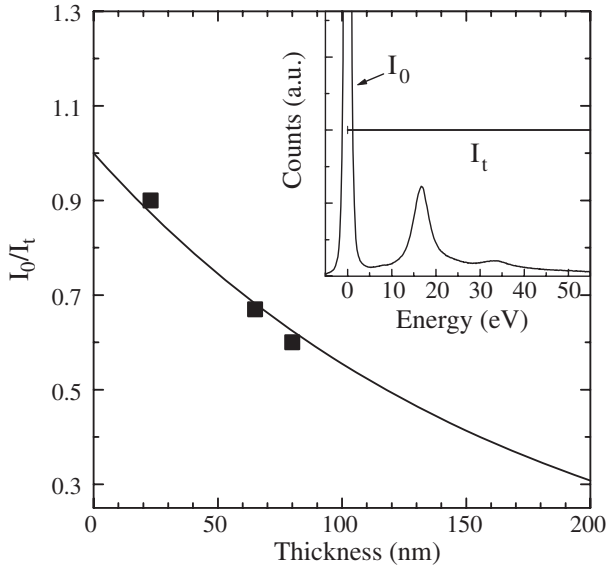

Figure 7. Ratio between the integral intensity of the zero-loss peak I_0 and the integral intensity I_t of the whole EELS spectrum as a function of the analysed thickness for the different studied materials. Data have been fitted with an exponential decreasing curve. In the inset the EELS spectrum of an amorphous Si film is shown. From the logarithm of the ratio between I_0 and I_t it is possible to estimate the thickness of the sample in electron mean free path units.

demonstrated that in some cases the crystalline core of the nc is surrounded by a bright shell, about 1 nm thick, characterized by the absence of lattice planes [22, 31].

Since EFTEM is able to detect the whole cluster population, it is possible to calculate the number of nanoclusters per unit volume at the different temperatures. However, in order to evaluate the density an accurate determination of the analysed volume is mandatory. This, in turn, makes necessary the availability of an estimation of the thickness sampled by the EFTEM experiment. The EELS technique provides a convenient way to estimate the local thickness of the analysed sample by a straightforward integration of the EELS signal. The intensity I_0 of the zero-loss peak, for a specimen of thickness t, is given by

$$I_0 = I_t \exp(-t/\lambda) \tag{1}$$

where I_t is the total area under the whole spectrum and λ is the mean free path for inelastic scattering [32].

With the purpose of measuring the local thickness, for each analysed EFTEM plan view image we have also collected an EELS spectrum. The ratio I_0/I_t between the integral intensity of the zero-loss peak I_0 and the integral intensity I_t of the whole EELS spectrum gives the thickness in electron mean free path (λ) units (see the inset of figure 7). To convert this number into depth units we need a reliable value of λ corresponding to our experimental conditions. This value has been determined by extracting in plan view configuration some EELS spectra from regions in which the whole thickness of amorphous Si, SiO_x and SiO_2 layers (having a thickness ranging from 25 to 80 nm) is analysed. The dependence of the experimentally evaluated I_0/I_t ratios on the thickness has been fitted with a decreasing exponential law for all the studied materials (see figure 7). In this way, we have found that the mean free path λ (corresponding to $I_0/I_t = 1/e$) of 200 kV electrons is equal to about 160 nm. Note that

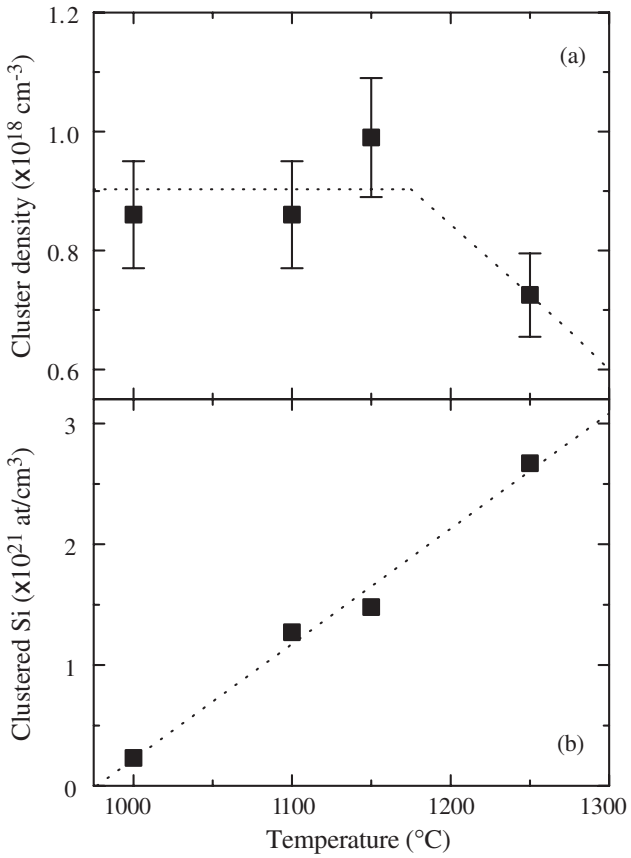

Figure 8. (a) Density of Si nanoclusters obtained from EFTEM images, and (b) concentration of clustered Si atoms (obtained from the data shown in figures 5 and 8(a)). The lines are drawn to guide the eye.

this value is almost independent of the film composition (as far as Si, SiO_2 and various SiO_x compositions are concerned) and it is in good agreement with other literature reports [33].

The EFTEM analyses for density measurements have been carried out in thin portions of the sample to avoid overlap among clusters. The density has been evaluated by counting the number of clusters displayed in each EFTEM image and by multiplying the image area by the local thickness obtained from the analysis of the EELS spectrum. The values for the Si nanocluster density we have obtained are reported in figure 8(a) as a function of the annealing temperature. The nanocluster density is almost constant in the 1000–1150 °C range (9×10^{17} cm^{-3}), while it decreases (about 7×10^{17} cm^{-3}) by increasing the annealing temperature up to 1250 °C. This result, coupled with the continuous increase in cluster size with annealing temperature reported in figure 5, suggests that nanocluster growth is not simply due to the inclusion of Si atoms diffusing from the oxide matrix, but Ostwald ripening effects, leading to the disappearance of small clusters, are probably also operating.

From the above reported data on the nanocluster density and mean radius the number of clustered Si atoms per unit volume at the different temperatures can be easily calculated. The obtained data are reported in figure 8(b) and demonstrate that the number of Si atoms forming detectable clusters remarkably increases by increasing the annealing temperature. In particular,

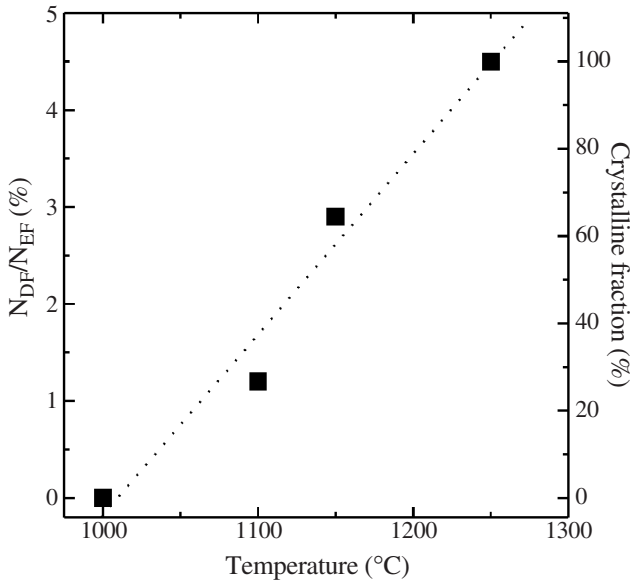

Figure 9. N_{DF}/N_{EF} ratio and crystalline fraction as a function of the annealing temperature for a fixed time of 1 h obtained from the comparison of EFTEM and DFTEM images. The line is drawn to guide the eye.

this value is about 2×10^{20} cm^{-3} at 1000 °C, and it increases by more than one order of magnitude (3×10^{21} cm^{-3}) by increasing the temperature up to 1250 °C, while intermediate values are seen at 1100 and 1150 °C. It is noteworthy that a relevant fraction of excess Si atoms not detectable by EFTEM exists even at 1250 °C. Indeed, the value of 3×10^{21} cm^{-3} has to be compared with an expected value for the excess Si content (by taking into account the total Si concentration of 46 at.% deduced from RBS measurements) of about 1×10^{22} cm^{-3}. On the basis of the present data, it is not possible to unambiguously determine if the missing Si atoms are embedded in clusters too small to be detected by TEM (clusters having a radius lower than 1 nm can be hardly detected also by using EFTEM), or if they are still dissolved in the SiO_x matrix. The existence of this 'invisible' fraction of Si atoms has to be taken into account when the density data of figure 8(a) are discussed. Indeed, the existence of a wide temperature range (1000–1150 °C) in which the cluster density seems to be almost constant is probably the result of a balance between the 'appearance' of new clusters (we cannot distinguish if this is due to the growth of smaller ones, or to the nucleation of new ones) and the 'disappearance' of small clusters due to ripening effects. On the other hand, at 1250 °C the Si atoms dissolved in the matrix or forming undetectable clusters are strongly diminished, and therefore ripening effects become more marked.

For samples in which the amorphous and crystalline phases coexist, we have estimated the crystalline fraction. In order to do this, the ratio between the number N_{DF} of ncs detected by DFTEM and the number N_{EF} of clusters detected by EFTEM has been evaluated. The cluster count has been performed in the same sample region for both techniques; shadowing effects among clusters placed at different depths have been minimized by analysing very thin regions. The data have been reported in figure 9, and a clear trend, showing the progressive increase of the N_{DF}/N_{EF} ratio by increasing the temperature, has been found.

Although it could be reasonable to assume that the value of 4.5% we have found for the N_{DF}/N_{EF} ratio at 1250 °C corresponds to a crystalline fraction of 100%, due to the very

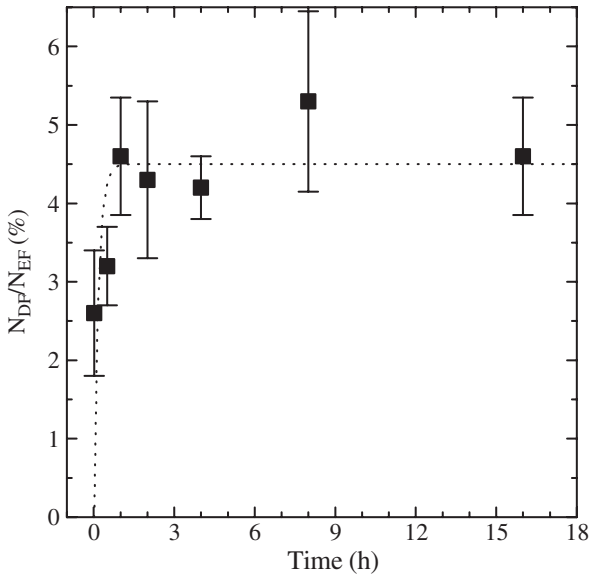

Figure 10. N_{DF}/N_{EF} ratio as a function of the annealing time for a fixed temperature of 1250 °C obtained from the comparison of EFTEM and DFTEM images. The line is drawn to guide the eye.

high annealing temperature, to unambiguously convert the data of figure 9 into a crystalline fraction further experimental evidence is needed. Since annealing temperatures above 1250 °C are hardly acceptable, also in view of possible industrial application of these materials, we have performed a series of thermal treatments in which, for a fixed temperature of 1250 °C, the annealing time varies from 1 min to 16 h. For such samples the N_{DF}/N_{EF} ratio has been evaluated and the results obtained are reported in figure 10. The data demonstrate that the transition from the amorphous to the crystalline phase is already present after only 1 min of annealing at 1250 °C and it is definitely completed after 1 h. Indeed, for annealing times equal or longer than 1 h, the value of the ratio N_{DF}/N_{EF} is almost constant to about 4.5%. This evidence, coupled with the fact that the value of 4.5% of the ratio N_{DF}/N_{EF} corresponds to the expected value for the fraction of crystals detected by DF in a fully crystalline sample under our experimental conditions [34], allows us to turn this value of 4.5% into a crystalline fraction of 100% and, by applying a simple criterion of proportionality, to evaluate the crystalline and the amorphous fraction in all cases where the two phases coexist (see the right-hand scale of figure 9).

Under the hypothesis that at 1250 °C all clusters are crystalline, the estimation of the nc fraction at lower temperatures leads to values of about 30% at 1100 °C (the temperature at which the crystallization process starts) and 60% at 1150 °C, clearly demonstrating that in this range, the temperature plays a role not only in inducing the cluster growth (i.e. in the increase of their mean radius), but also in extensively promoting the amorphous to crystal transition [26].

Finally, we have used the data on the Si nanocluster density reported in figure 8(a) and those on the crystalline fraction reported in figure 9 to calculate the concentration of nc and of na as a function of the annealing temperature. The obtained data are reported in figure 11 and demonstrate that the temperature progressively induces the transformation of 9×10^{17} na cm^{-3} into 7×10^{17} nc cm^{-3}, with the loss of about 20% of the clusters present at 1000 °C, due to the above discussed occurrence of Ostwald ripening phenomena.

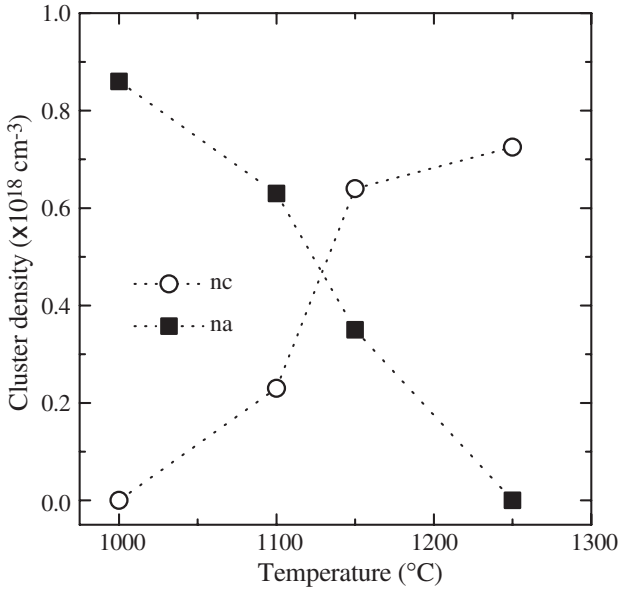

Figure 11. Density of amorphous (na) and crystalline (nc) nanoclusters (obtained from the data shown in figures 8(a) and 9), as a function of the annealing temperature. The lines are drawn to guide the eye.

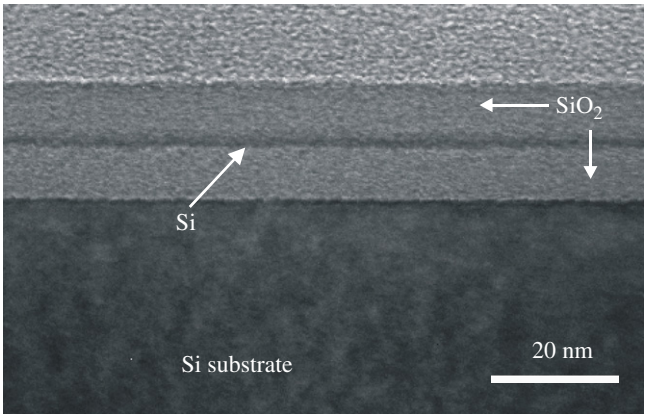

Figure 12. Bright field TEM cross section of the as deposited $SiO_2/Si/SiO_2$ structure.

3.2. Si nanoclusters from Si/SiO$_2$ multilayers

The structure of the as deposited $SiO_2/Si/SiO_2$ multilayer is shown in the bright field TEM cross section reported in figure 12. The Si layer appears homogeneous and continuous. It was not possible to observe any electron diffraction pattern corresponding to the presence of a crystalline phase for this sample, demonstrating the amorphous nature of the Si layer. Also for this system we have collected plan view EFTEM Si maps, by using a 4 eV wide energy window centred in correspondence to the Si plasmon loss peak at about 17 eV, to monitor the thermal evolution of the system. The EFTEM plan view micrograph of the as deposited sample confirms the homogeneous nature of the Si layer. EFTEM images demonstrate the absence

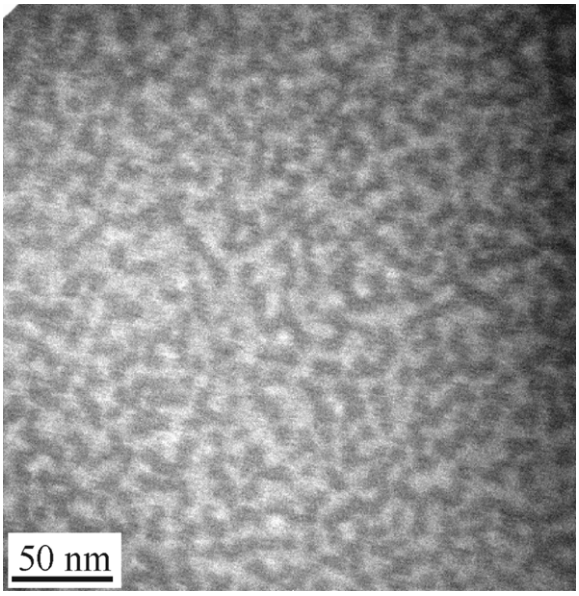

Figure 13. EFTEM plan view image of a SiO_2/Si/SiO_2 multilayer annealed at 1000 °C for 1 h.

of any relevant clustering effect up to 900 °C. On the other hand, the EFTEM micrograph of the sample annealed at 1000 °C for 1 h, reported in figure 13, shows the formation of a Si network (the bright part of the image) as opposed to the initial continuous layer. The reason for this phenomenon could be a thermal grooving induced by the presence of the subnanometric roughness typical of PECVD prepared films. It is well known that roughness can develop in thin films during high temperature annealing, originating a grooving process [35]. This effect can extensively modify the structure of the whole film if the roughness is of the same order of magnitude of the thickness. During high temperature annealing of the Si layers, Si atoms may diffuse away from the regions of high curvature. This phenomenon leads to the breaking of the layer; once the breaking is started, the process continues until constant curvature surfaces are formed, and, as a consequence, as can be seen in figure 14(a), at 1100 °C the first well defined spherical clusters are detected by EFTEM. However, the highly interconnected Si structure visible at 1000 °C is still partially present. At 1200 °C (see the EFTEM image of figure 14(b)) the breaking of the Si layer is almost completed and most of the nanoclusters have a well defined spherical shape. Finally, as shown by the EFTEM plan view image of figure 14(c), a system characterized by almost spherical and well separated nanoclusters is achieved at 1250 °C. Note finally that also the different surface energy between Si and SiO_2 can help us to explain the final morphology of the system. The surface energy determines whether, at the equilibrium, one material wets another and forms an uniform adherent layer [36]. SiO_2 has a low surface energy while Si has a high surface energy. This means that the Si layer tends to ball up, in order to reduce the interface with SiO_2 and minimize the surface energy.

Transmission electron diffraction measurements reveal that the samples annealed up to 1000 °C are amorphous. On the other hand, the diffraction pattern shows the characteristic rings due to the presence of Si ncs for the samples annealed at 1100, 1200 and 1250 °C for 1 h. The evidence of the crystallization after annealing processes at 1100 °C or higher allows us to carry out DFTEM analyses. The more striking result is found when we make a comparison between the EFTEM image of the sample annealed at 1100 °C for 1 h, shown in figure 14(a),

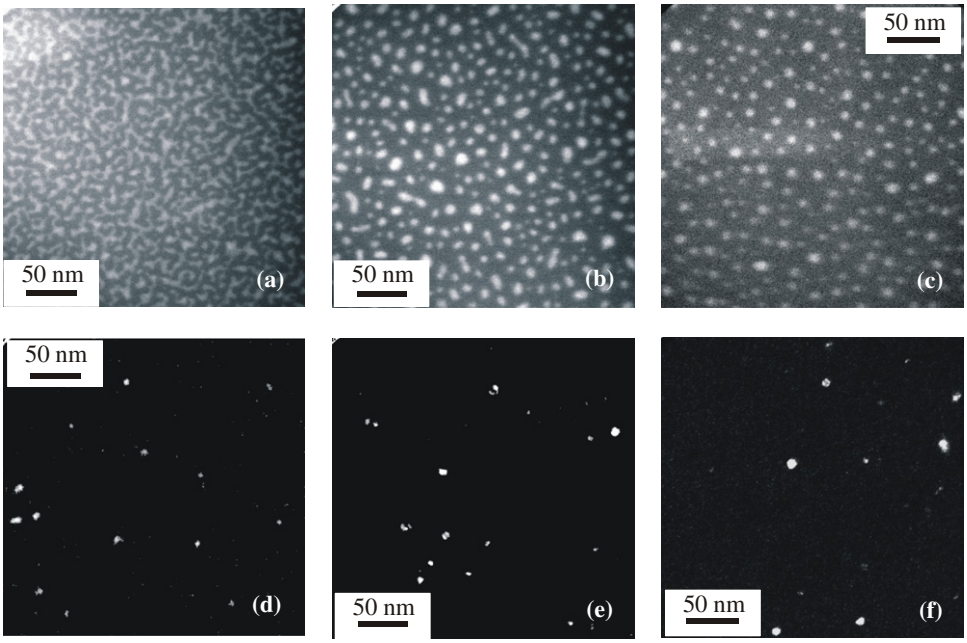

Figure 14. EFTEM plan view images of $SiO_2/Si/SiO_2$ structures after annealing processes at (a) 1100 °C, (b) 1200 °C, and (c) 1250 °C for 1 h. DFTEM plan view images of $SiO_2/Si/SiO_2$ structures after annealing processes at (d) 1100 °C, (e) 1200 °C and (f) 1250 °C for 1 h.

and the DFTEM image of the same sample, shown in figure 14(d). Indeed, the DFTEM image suggests the presence of almost spherical and isolated Si ncs, but this view is a very partial aspect of the complex structure evidenced by the corresponding EFTEM image. On the other hand, figures 14(e) and (f) report the DFTEM images of the samples annealed at 1200 and 1250 °C for 1 h; from the comparison with the corresponding EFTEM images, we conclude that in these cases both techniques give us a very similar structural picture, the only relevant differences between the two kinds of images being in the number of detected clusters that, in agreement with the considerations reported in the previous section, is remarkably higher for the EFTEM images.

The structural evolution of the $SiO_2/Si/SiO_2$ multilayers has also been studied as a function of the annealing time for a fixed temperature of 1100 °C. Figure 15 reports the plan view EFTEM images corresponding to $SiO_2/Si/SiO_2$ samples after thermal processes of 30 min (figure 15(a)) and 8 h (figure 15(b)) at 1100 °C. It can be noted that, already after a 30 min process, an extensive breaking of the Si layer is observed; however, the agglomeration process exhibits a very slow kinetics; indeed, as shown in figure 15(b), even after an 8 h process, large and interconnected Si nanostructures predominate over the small and spherical ones.

As already extensively discussed in the previous section, the comparison between DF and EF images allows the evaluation of the crystalline fraction. The data we have obtained for the $SiO_2/Si/SiO_2$ system, reported in figure 16(a), demonstrate the progressive increase of the crystalline fraction by increasing the temperature, from about 10% at 1100 °C to 90% at 1200 °C and 100% at 1250 °C. Note that the almost complete crystallization of the ultra-thin Si layer requires the use of temperatures as high as 1200 °C. Indeed, figure 16(b), reporting the crystalline fraction as a function of the annealing time for a fixed temperature of 1100 °C,

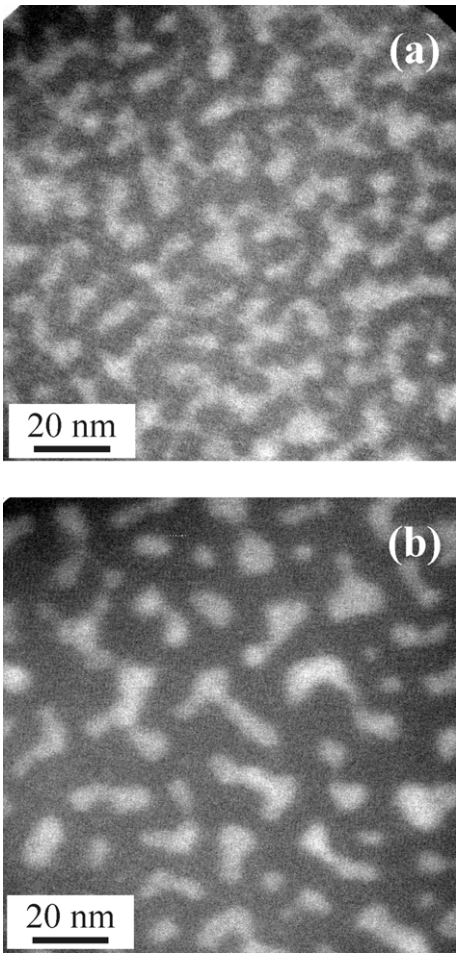

Figure 15. EFTEM plan view images of $SiO_2/Si/SiO_2$ structures after annealing processes at 1100 °C for (a) 30 min and (b) 8 h.

demonstrates that the kinetics of crystallization at 1100 °C is extremely slow, since even after an 8 h process the crystalline fraction remains lower than 20%.

3.3. Correlation between structural and optical properties of Si nanoclusters

Figure 17(a) reports the PL spectra taken at room temperature from SiO_x films having a total Si concentration of 46 at.% by pumping with the 488 nm line of an Ar^+ laser, after thermal annealing processes performed at temperatures ranging from 1000 to 1250 °C. As deposited SiO_x films exhibit only broad and very weak PL signals, possibly related to the presence of radiative defects in the matrix. A relatively weak PL signal at about 900 nm (not shown) has been observed for films annealed at 900 °C. On the other hand, the figure shows that the annealed SiO_x samples exhibit strong PL signals; the wavelength corresponding to the maximum of the emission is about 900 nm, almost independently of the annealing temperature. The reasons for such a weak variation of the emitted wavelength in samples characterized by very different Si nc mean radii have been already discussed [22]. On the other hand, figure 17(a)

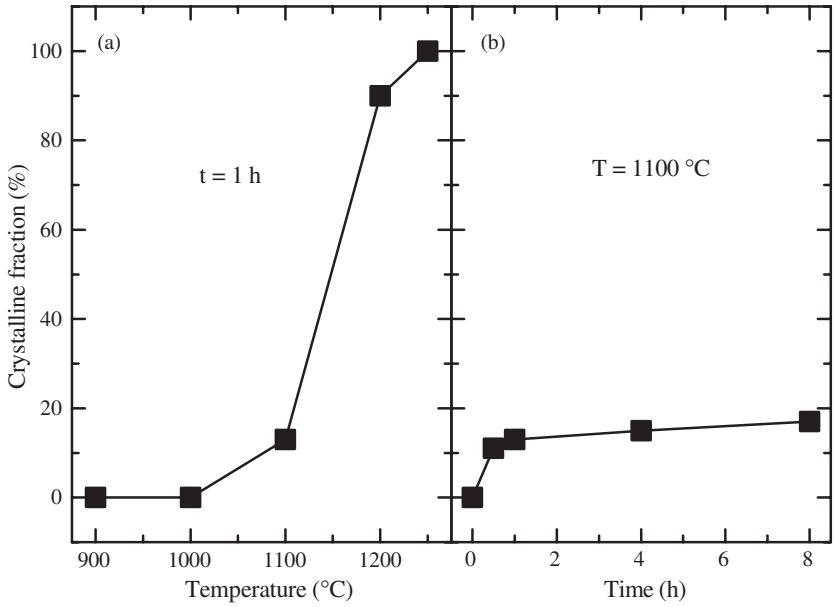

Figure 16. Crystalline fraction for $SiO_2/Si/SiO_2$ structures as a function of (a) the annealing temperature for a fixed process time of 1 h and (b) the annealing time for a fixed temperature of 1100 °C.

demonstrates that the annealing temperature strongly influences the PL intensity, that increases by a factor of 15 by increasing the temperature from 1000 to 1150 °C. A further increase of the temperature up to 1250 °C leads to a decrease of the PL intensity by a factor of 3.

We have also studied the PL properties of ten-period Si/SiO_2 structures having the same Si and SiO_2 thicknesses as the $SiO_2/Si/SiO_2$ samples analysed by EFTEM. The use of such a ten-period structure has been chosen to maximize the intensity of the PL signal. No relevant PL signals have been detected from samples annealed below 1100 °C, while, as shown in figure 17(b), intense peaks in the 700–1100 nm region are observed for samples annealed at 1100, 1200 and 1250 °C for 1 h. PL intensity has its maximum value at 1200 °C. The PL signal shifts from 850 nm, for the sample annealed at 1100 °C, to 940 nm, for the sample annealed at 1250 °C. The spectrum taken from the sample annealed at 1100 °C also presents a peak centred at about 1140 nm due to the Si substrate excitation.

In the low pump power regime, the PL intensity I is given by

$$I \propto \sigma\phi\frac{\tau}{\tau_R}N \tag{2}$$

where τ is the lifetime, τ_R is the radiative lifetime, σ is the excitation cross section, ϕ is the photon flux and N is the total number of emitting centres. According to equation (2), for the same excitation conditions, the PL intensity depends only on the lifetime τ and on the total number of emitting centres N. Therefore, in order to correlate the optical and the structural properties, we also need to measure the lifetime of the PL signal. These measurements have been made by studying the decay time of the PL signal recorded at 850 nm after shutting off the pumping laser beam. The data are reported in figure 18 for the case of SiO_x films annealed at different temperatures; a very fast lifetime is found for samples annealed at 1000 °C, while it becomes remarkably slower by increasing the annealing temperature. In the temperature range

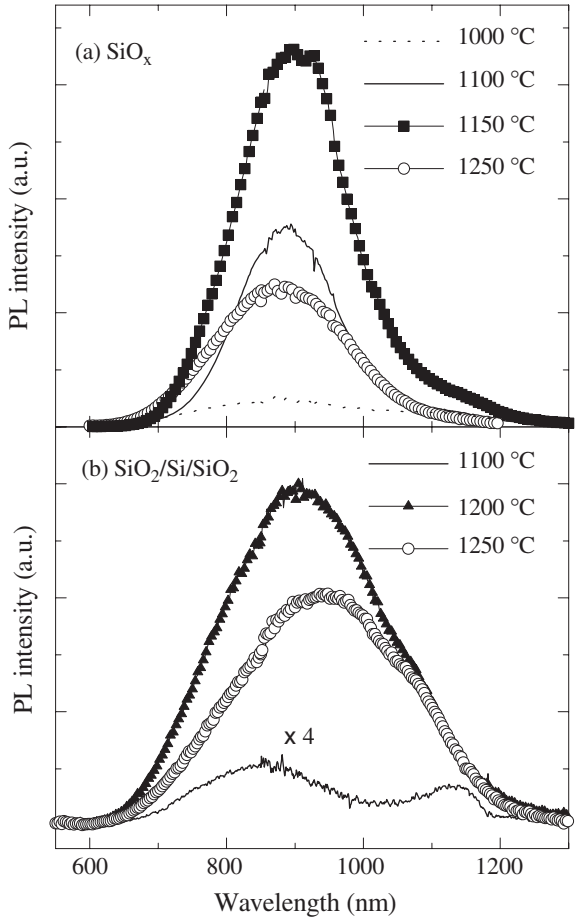

Figure 17. Room temperature PL spectra obtained with an excitation wavelength of 488 nm. (a) SiO_x films annealed at different temperatures for 1 h; (b) Si/SiO_2 multilayers annealed at different temperatures for 1 h.

from 1100 to 1250 °C the PL signal decay is characterized by a stretched exponential shape, given by

$$I(t) = I_0 \exp\left[-\left(\frac{t}{\tau}\right)^{\beta}\right] \tag{3}$$

where $I(t)$ and I_0 are the PL intensities as a function of time and at $t = 0$ and β is a dispersion factor $\leqslant 1$; β values equal to 1 (corresponding to single exponential decays) have been observed in systems in which interactions among Si ncs are very weak, while β values lower than 1 characterize the decay of interacting Si ncs [25, 37, 38]. By fitting the experimental curves reported in figure 18 with equation (3), we have found that by increasing the annealing temperature in the range 1100–1250 °C the lifetime slightly increases from 20 to about 30 μs and β increases from 0.62 to 0.71. On the other hand, the decay curve relative to the sample annealed at 1000 °C exhibits a more complex behaviour, and it cannot be fitted by using equation (3), since it is possible in such a curve to identify two very different components, a first one corresponding to a very fast decay, having a lifetime shorter than 1 μs, and a second slower component, resembling for long decay times that relative to the samples annealed at

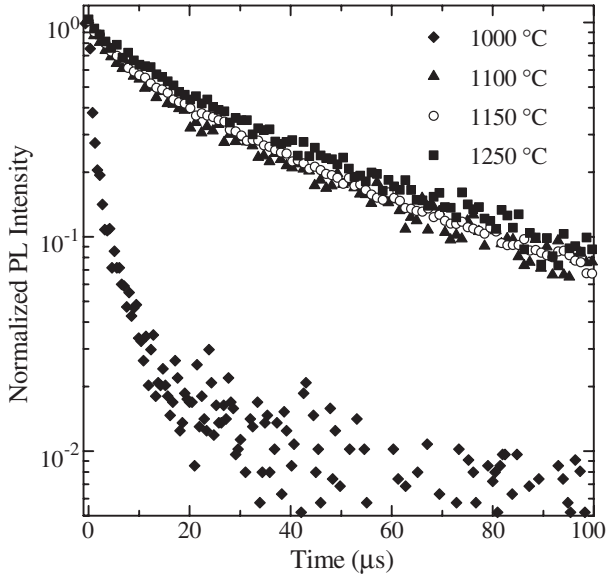

Figure 18. Decay time of the room temperature PL signal recorded at 850 nm for SiO_x films annealed at different temperatures for 1 h.

higher temperatures. This fast component of the lifetime is reasonably related to the presence of non-radiative recombination centres in the oxide matrix or within the clusters, due to the relatively low temperature of the annealing process.

In the case of Si/SiO_2 multilayers the lifetime of the PL signals is well described by a stretched exponential function for all the studied temperatures. By fitting the experimental curves (not shown) with equation (3), we have found that by increasing the annealing temperature in the range 1100–1250 °C the lifetime increases from 15 to 70 μs and the dispersion factor β increases from 0.66 to 0.77.

For the case of annealed SiO_x films the normalized number N of emitting Si nanoclusters, as obtained from equation (2) by dividing the PL intensity I by the lifetime τ (and assuming an almost constant τ_R) is reported in arbitrary units in figure 19(a) (solid squares) as a function of the annealing temperature. From the comparison between these data and the density of amorphous and crystalline clusters and their sum, reported in figures 8(a) and 11, it is possible to draw some interesting conclusions about the relationship between structural and optical properties of Si nanoclusters embedded in SiO_2 films. Figure 19(a) also reports (open circles) the normalized cluster density taken from the EFTEM data (i.e. the sum of the amorphous and crystalline contributions), as a function of the annealing temperature. The figure demonstrates that there is a good agreement between the two sets of data. At 1250 °C the number of emitting centres is more than a factor of two lower than the nanocluster density, and this is due to the fact that at this temperature the nanocluster mean radius is very high (2.6 nm), and since size distributions are typically characterized by a standard deviation of about 20%, a relevant fraction of the Si clusters is too large to be a good light emitter. Indeed, according to the effective mass approximation model [39], only clusters having a radius remarkably lower than the Bohr radius of the exciton (about 5 nm for bulk Si), exhibit strong quantum confinement effects [40]. It is not possible to find a better agreement by correlating the PL data with only the amorphous fraction (it should be impossible to explain the PL signal at 1250 °C in a fully

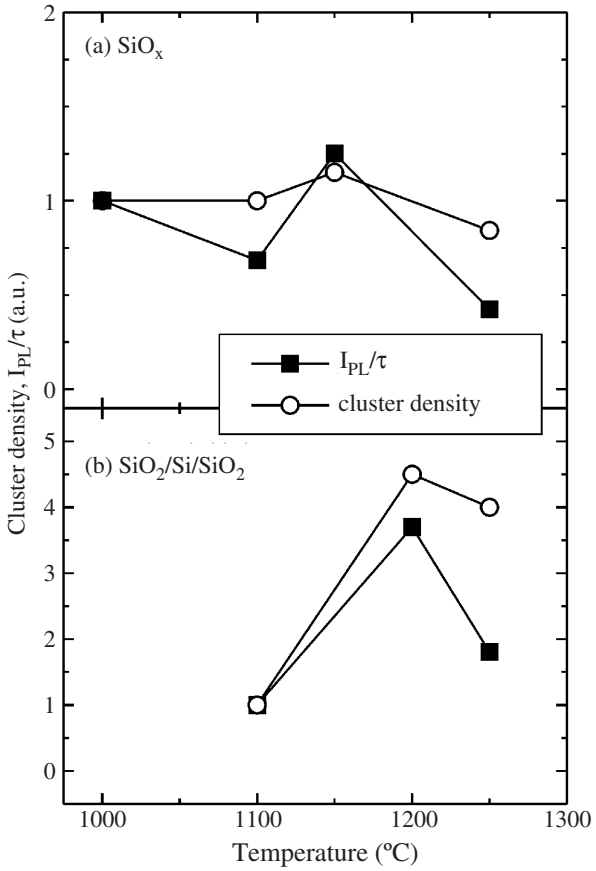

Figure 19. Concentration N of emitting Si nanoclusters, as obtained from equation (2) by dividing the integrated PL intensity I by the lifetime τ (solid squares) and Si nanocluster density (open circles) taken from EFTEM data, as a function of the annealing temperature for a fixed process time of 1 h for (a) SiO_x films and (b) Si/SiO_2 multilayers. The data in (a) are normalized to their respective values at 1000 °C, while data in (b) are normalized to their respective values at 1100 °C.

crystalline sample) or the crystalline fraction (the maximum PL intensity should be at 1250 °C and no PL signal should appear at 1000 °C).

The above approach has also been used for the Si/SiO_2 multilayers. Since the clusters formed by the thermal annealing are dispersed on a single layer, the EFTEM data shown in the previous section allow a straightforward evaluation of their density. For the sample annealed at 1100 °C for 1 h the density of the well defined clusters is about 6.7×10^{10} cm^{-2}. The density strongly increases to 3.0×10^{11} cm^{-2} at 1200 °C (with a mean radius of 3.7 nm), while a slightly lower value of 2.7×10^{11} cm^{-2} is observed at 1250 °C (mean radius of 4.1 nm). This small variation arises from the balance of two different simultaneous phenomena, i.e. the formation of new spherical clusters, due to the breaking of the irregular clusters present at 1200 °C and a conservative Ostwald ripening phenomenon, leading to the formation of large clusters at the expenses of smaller ones, as also evidenced by the analysis of the tails of the size histograms.

As discussed above, in the low pump power regime the number of emitting centres can be obtained by the ratio between the integrated PL intensity and the lifetime of the PL signal.

The nanocluster density (open circles) and the number of emitting centres (solid squares), normalized to their respective values at 1100 °C, are reported in figure 19(b) as a function of the temperature. It is noteworthy that also in this case the two curves exhibit the same behaviour, demonstrating that the appearance of a strong PL from annealed Si/SiO_2 multilayers is due to Si nanocluster formation. Note that at 1250 °C the actual cluster density is higher than the number of emitting centres (i.e. the PL signal is weaker than expected on the basis of the structural data) because at this temperature a considerable fraction of the clusters has a size remarkably higher than the Bohr radius of the exciton, and therefore gives a negligible contribution to the PL signal.

Also the obtained values for the PL lifetime and for the dispersion factor β, and their dependence on the annealing temperature, can be fully understood by using the TEM data. The comparison between EFTEM and DFTEM images suggests that most of the well defined clusters formed at 1100 °C are crystalline. For these clusters the edge-to-edge mean on-plane distance from the surrounding aggregates is about 3.5 nm, a value remarkably lower than the distance along the growth direction (7 nm, as determined by the SiO_2 spacer thickness). Under optical pumping, this determines an energy flow from the small clusters to the larger and partially interconnected structures shown in figure 14(a), which may act as centres for non-radiative recombination, leading to a fast decay time of 15 μs. In agreement with this picture, the low value (0.66) of the dispersion factor β confirms the presence of a strong interaction among nanoclusters [25, 37, 38]. On the other hand, at 1250 °C samples can be considered fully crystalline. The interaction among clusters is strongly reduced (the edge-to-edge mean distance on the plane is about 11 nm), with the consequence that they behave as efficient light emitters. The increased PL lifetime confirms the suppression of non-radiative paths. Note finally that the observation of a β value of 0.77, although larger than that found for samples treated at 1100 °C, may be considered surprising if compared with the very large distance among adjacent clusters. To explain this effect we have to recall that the inter-plane distance is 7 nm, i.e. remarkably lower than the on-plane distance, and therefore in this case an interaction between clusters lying on different planes may occur [25].

4. Conclusions

The comparative analysis of EFTEM and DFTEM data has highlighted the structure of SiO_x films and $SiO_2/Si/SiO_2$ multilayers within a wide range of annealing processes. As deposited SiO_x films are homogeneous and fully amorphous materials, without any evidence of phase separation; the first steps of the phase separation between Si and SiO_2 become visible at 900 °C, but well defined amorphous Si clusters are formed only at 1000 °C. At 1100 °C the amorphous clusters start to become crystalline, and the crystalline fraction increases by further increasing the annealing temperature. Furthermore, the capability of the EFTEM technique to detect all the Si clusters, independently of their crystalline state, has allowed us to make a very reliable determination of the Si nanocluster mean radius and density as a function of the annealing temperature. Finally, the availability of a much more complete quantitative picture allowed the demonstration that amorphous Si clusters constitute a relevant fraction of the overall population in samples annealed at intermediate temperatures and also play a fundamental role in determining the PL properties of the system. For the case of ultra-thin Si layers it has been demonstrated that the first step of the layer modification consists in the formation of a highly interconnected Si structure. The progressive breaking of this structure leads to the formation of Si ncs embedded in SiO_2, and, in turn, to the appearance of a strong PL signal, quantitatively related to the Si nc concentration. The above new evidence constitutes

a relevant tool for a full comprehension of the properties of Si nanostructures and for their application for the development of a Si-based optoelectronics.

Acknowledgments

The authors want to thank N Marino, S Pannitteri, and A Spada for their expert technical collaboration. This work has been partially supported by MIUR through the projects FIRB and D.D. 1105.

References

[1] Pavesi L, Dal Negro L, Mazzoleni C, Franzò G and Priolo F 2000 *Nature* **408** 440
[2] Khriachtchev L, Rasanen M, Novikov S and Sinkkonen J 2001 *Appl. Phys. Lett.* **79** 1249
[3] Luterova K, Pelant I, Mikulskas I, Tomasiunas R, Muller D, Grob J-J, Rehspringer J-L and Honerlage B 2002 *J. Appl. Phys.* **91** 2896
[4] Dal Negro L, Cazzanelli M, Pavesi L, Ossicini S, Pacifici D, Franzò G, Priolo F and Iacona F 2003 *Appl. Phys. Lett.* **82** 4636
[5] Ruan J, Fauchet P M, Dal Negro L, Cazzanelli M and Pavesi L 2003 *Appl. Phys. Lett.* **83** 5479
[6] Cazzanelli M, Navarro-Urrios D, Riboli F, Daldosso N, Pavesi L, Heitmann J, Yi L X, Scholz R, Zacharias M and Gosele U 2004 *J. Appl. Phys.* **96** 3164
[7] Dal Negro L, Cazzanelli M, Danese B, Pavesi L, Iacona F, Franzò G and Priolo F 2004 *J. Appl. Phys.* **96** 5747
[8] Qin G G, Li A P, Zhang B R and Li B-C 1995 *J. Appl. Phys.* **78** 2006
[9] Hirschman K D, Tsybeskov L, Duttagupta S P and Fauchet P M 1996 *Nature* **384** 338
[10] Rebohle L, von Borany J, Yankov R A, Skorupa W, Tyschenko I E, Frob H and Leo K 1997 *Appl. Phys. Lett.* **71** 2809
[11] Fujita S and Sugiyama N 1999 *Appl. Phys. Lett.* **74** 308
[12] Lalic N and Linnros J 1999 *J. Lumin.* **80** 263
[13] Photopoulos P and Nassiopoulou A G 2000 *Appl. Phys. Lett.* **77** 1816
[14] Franzò G, Irrera A, Moreira E C, Miritello M, Iacona F, Sanfilippo D, Di Stefano G, Fallica P G and Priolo F 2002 *Appl. Phys.* A **74** 1
[15] Irrera A, Pacifici D, Miritello M, Franzò G, Priolo F, Iacona F, Sanfilippo D, Di Stefano G and Fallica P G 2002 *Appl. Phys. Lett.* **81** 1866
[16] Irrera A, Iacona F, Crupi I, Presti C D, Franzò G, Bongiorno C, Sanfilippo D, Di Stefano G, Piana A, Fallica P G, Canino A and Priolo F 2006 *Nanotechnology* **17** 1428
[17] Arnoldbik W M, Tomozeiu N, van Hattum E D, Lof R W, Vredenberg A M and Habraken F H P M 2005 *Phys. Rev.* B **71** 125329
[18] Song H Z, Bao X M, Li N S and Wu X L 1998 *Appl. Phys. Lett.* **72** 356
[19] Kenyon A J, Trwoga P F, Pitt C W and Rehm G 1996 *J. Appl. Phys.* **79** 9291
[20] Inokuma T, Wakayama Y, Muramoto T, Aoki R, Kurata Y and Hasegawa S 1998 *J. Appl. Phys.* **83** 2228
[21] Iacona F, Franzò G and Spinella C 2000 *J. Appl. Phys.* **87** 1295
[22] Iacona F, Bongiorno C, Spinella C, Boninelli S and Priolo F 2004 *J. Appl. Phys.* **95** 3723
[23] Tsybeskov L, Hirschman K D, Duttagupta S P, Zacharias M, Fauchet P M, McCaffrey J P and Lockwood D J 1998 *Appl. Phys. Lett.* **72** 43
[24] Photopoulos P, Nassiopoulou A G, Kouvatsos D N and Travlos A 2000 *Appl. Phys. Lett.* **76** 3588
[25] Vinciguerra V, Franzò G, Priolo F, Iacona F and Spinella C 2000 *J. Appl. Phys.* **87** 8165
[26] Zacharias M, Blasing J, Veit P, Tsybeskov L, Hirschman K D and Fauchet P M 1999 *Appl. Phys. Lett.* **74** 2614
[27] Boninelli S, Iacona F, Franzò G, Bongiorno C, Spinella C and Priolo F 2005 *Nanotechnology* **16** 3012
[28] Williams D B and Carter C B 1996 *Transmission Electron Microscopy* vol 1 (New York: Plenum)
[29] Philipp H R 1972 *J. Non-Cryst. Solids* **8–10** 627
[30] Iacona F, Lombardo S and Campisano S U 1996 *J. Vac. Sci. Technol.* B **14** 2693
[31] Daldosso N, Luppi M, Ossicini S, Degoli E, Magri R, Dalba G, Fornasini P, Grisenti R, Rocca F, Pavesi L, Boninelli S, Priolo F, Spinella C and Iacona F 2003 *Phys. Rev.* B **68** 085327
[32] Egerton R F 1996 *Electron Energy-Loss Spectroscopy in the Electron Microscope* 2nd edn (New York: Plenum)
[33] Bonafos C, Garrido B, Lopez M, Perez-Rodriguez A, Morante J R, Kihn Y, Ben Assayag G and Claverie A 2000 *Appl. Phys, Lett.* **76** 3962

[34] Crupi I, Lombardo S, Spinella C, Bongiorno C, Liao Y, Gerardi C, Fazio B, Vulpio M and Privitera S 2001 *J. Appl. Phys.* **89** 5552
[35] Nolan T P, Sinclair R and Beyers R 1992 *J. Appl. Phys.* **71** 720
[36] Tu K N, Mayer J W and Feldman L C 1992 *Electronic Thin Film Science for Electrical Engineers and Materials Scientists* (New York: Macmillian)
[37] Priolo F, Franzò G, Pacifici D, Vinciguerra V, Iacona F and Irrera A 2001 *J. Appl. Phys.* **89** 264
[38] Linnros J, Lalic N, Galeckas A and Grivickas V 1999 *J. Appl. Phys.* **86** 6128
[39] Efros Al L and Efros A L 1982 *Sov. Phys.—Semicond.* **16** 772
[40] Trwoga P F, Kenyon A J and Pitt C W 1998 *J. Appl. Phys.* **83** 3789